Published in final edited form as:
Cell Host Microbe. 2013 February 13; 13(2): . doi:10.1016/j.chom.2013.01.009.

The Herpesvirus VP1/2 Protein Is an Effector of Dynein-Mediated Capsid Transport and Neuroinvasion

Sofia V. Zaichick[1], **Kevin P. Bohannon**[1], **Ami Hughes**[1], **Patricia J. Sollars**[2], **Gary E. Pickard**[2,3], and **Gregory A. Smith**[1,*]

[1]Department of Microbiology-Immunology, Northwestern University Feinberg School of Medicine, Chicago, IL 60611, USA

[2]School of Veterinary Medicine and Biomedical Sciences, University of Nebraska-Lincoln, Lincoln, NE 68583, USA

[3]Department of Ophthalmology and Visual Sciences, University of Nebraska Medical Center, Omaha, NE 68198, USA

SUMMARY

Microtubule transport of herpesvirus capsids from the cell periphery to the nucleus is imperative for viral replication and, in the case of many alphaherpesviruses, transmission into the nervous system. Using the neuroinvasive herpesvirus, pseudorabies virus (PRV), we show that the viral protein 1/2 (VP1/2) tegument protein associates with the dynein/dynactin microtubule motor complex and promotes retrograde microtubule transport of PRV capsids. Functional activation of VP1/2 requires binding to the capsid protein pUL25 or removal of the capsid-binding domain. A proline-rich sequence within VP1/2 is required for the efficient interaction with the dynein/dynactin microtubule motor complex as well as for PRV virulence and retrograde axon transport in vivo. Additionally, in the absence of infection, functionally active VP1/2 is sufficient to move large surrogate cargoes via the dynein/dynactin microtubule motor complex. Thus, VP1/2 tethers PRV capsids to dynein/dynactin to enhance microtubule transport, neuroinvasion, and pathogenesis.

INTRODUCTION

Upon entering a host cell, many viruses move centripetally along microtubules to reach sites of replication. Although the dynein/ dynactin motor complex is implicated in the transport of viruses at this early step of infection, molecular events underlying viral recruitment of dynein/dynactin remain poorly defined (reviewed in Dodding and Way, 2011). Understanding the biology of dynein-based transport is particularly important for the study of neuroinvasive herpesviruses such as herpes simplex virus (HSV) and varicella zoster virus. While the high incidence of neuroinvasive herpesvirus infections is primarily attributed to the propensity of these agents to establish latent infections, latency establishment is contingent on retrograde axon transport to neuronal soma, a process dependent upon dynein/dynactin recruitment to the herpesvirus capsid.

*Correspondence: g-smith3@northwestern.edu.

SUPPLEMENTAL INFORMATION

Supplemental Information includes three figures, three tables, Supplemental Experimental Procedures, and one movie and can be found with this article online at http://dx.doi.org/10.1016/j.chom.2013.01.009.

Pseudorabies virus (PRV) is a veterinary herpesvirus noted for its pronounced neuroinvasion and virulence in many mammalian hosts (Enquist, 1994). Like other neuroinvasive herpesviruses, PRV transports on axonal microtubules to deliver its genetic information to neurons in sensory ganglia (retrograde transport) and later to reemerge from the nervous system by spreading to innervated peripheral tissues (anterograde transport) (Bosem et al., 1990; Kristensson et al., 1986; Openshaw et al., 1978). Herpesviruses consist of an enveloped icosahedral capsid that contains tegument proteins between the capsid and envelope. Upon entering neurons, the outer components of the PRV virion, including the envelope and a subset of tegument proteins, are shed (Luxton et al., 2005). The remaining capsid-tegument entry complex participates in rapid microtubule-dependent retrograde transport (Antinone and Smith, 2010; Luxton et al., 2005). Evidence is accumulating that several proteins of the entry complex are effectors for early events leading up to the injection of the viral genome into the nucleus (Delboy and Nicola, 2011; Douglas et al., 2004; Krautwald et al., 2009; Rode et al., 2011). However, as is the case for most viruses, the specific viral proteins that engage the dynein/dynactin motor complex and enable minus-end-directed microtubule transport remain undefined.

Viral protein 1/2 (VP1/2; also called pUL36) is a large tegument protein bound directly to the capsid surface and a component of the capsid-tegument entry complex (Antinone and Smith, 2010; Cardone et al., 2012; Coller et al., 2007; Luxton et al., 2005). PRV deleted for the gene encoding VP1/2 fails to propagate, making functional studies of VP1/2 during early infection difficult (Fuchs et al., 2004; Smith and Enquist, 1999). Nevertheless, several studies have documented that VP1/2 is critical for delivery of incoming viral particles to nuclear pores and release of the viral DNA into the nucleus (Abaitua et al., 2012; Jovasevic et al., 2008; Roberts et al., 2009; Schipke et al., 2012). In this study we demonstrate that VP1/2 associates with the dynein motor and is a potent effector of microtubule-dependent transport that can function independently of other viral proteins to move cargo in cells. VP1/2 was expressed in an inert state in the absence of other viral proteins, but was activated either by coexpression with its binding partner, pUL25, or by removal of the pUL25 binding site in the VP1/2 C terminus. Additionally, several regions of VP1/2 contributed to binding of dynactin, a cellular complex that augments dynein-based microtubule transport. In particular, deletion of a large proline-rich sequence in VP1/2 reduced dynactin binding, axon transport in culture, and neuroinvasion in vivo. Based on these findings, we infer that VP1/2 is active when bound to the capsid surface where it recruits dynein/dynactin and promotes the sustained retrograde microtubule transport necessary to travel long distances in axons and invade the nervous system.

RESULTS

The C-Terminal Capsid-Binding Domain in VP1/2 Modulates Cellular Localization and Intracellular Transport

VP1/2 is a capsid-bound tegument protein and is the largest protein encoded by the herpesviridae (Gibson and Roizman, 1972). Approximately one-third of VP1/2 consists of proline-rich sequences that map to two regions of the protein (Figure 1A). Although the two proline-rich regions of VP1/2 ortho-logs of other alphaherpesviruses are positionally maintained, the primary sequences of the proline-rich regions are divergent between viruses. When transiently expressed in the absence of other viral proteins, a PRV RFP-VP1/2 fusion protein was diffusely distributed and was often nuclear enriched (Figure 1B). This distribution of VP1/2 is consistent with previous reports of transiently expressed HSV and PRV VP1/2 (Abaitua and O'Hare, 2008; Lee et al., 2006). During infection VP1/2 interacts with capsids through multiple points of contact with the capsid surface (Cardone et al., 2012). One domain of VP1/2 that contributes to the capsid interaction has been mapped to the 62 C-terminal amino acids, which are sufficient for capsid binding through an interaction

with the pUL25 capsid protein (Coller et al., 2007; Pasdeloup et al., 2009). Similar to VP1/2, a GFP-pUL25 fusion protein was diffusely distributed when transiently expressed, consistent with previous reports of HSV pUL25 (Ogasawara et al., 2001; Rode et al., 2011). In contrast, coexpression of RFP-VP1/2 and GFP-pUL25 resulted in redistribution of both proteins to the nuclear membrane and perinuclear region (Figure 1C). The intensity of nuclear rim localization was variable but was clearly evident in 28% (n = 97) of transfected cells; perinuclear localization was less frequent. The observed redistribution to the nuclear rim was often accompanied by a punctate pattern of fluorescence from the cytoplasm, which was subsequently determined to be motile (see below).

Capsid-VP1/2 complexes translocate to the nucleus upon entering cells (Antinone and Smith, 2010; Copeland et al., 2009; Jovasevic et al., 2008; Luxton et al., 2005; Morrison et al., 1998; Schipke et al., 2012). Therefore, the nuclear membrane localization of coexpressed VP1/2 and pUL25 was noteworthy. The mechanism underlying VP1/2-pUL25 redistribution could be intrinsic to either protein; however, we have previously noted that VP1/2 can localize to the nuclear membrane during PRV infection (Bohannon et al., 2012; Leelawong et al., 2012). Consistent with these observations, removal of the C-terminal pUL25 binding site from VP1/2 (VP1/2ΔR7) enhanced nuclear rim localization greater than 10-fold in the absence of pUL25, indicating that nuclear rim localization was an intrinsic property of VP1/2 (Figure 1D). These results predict that VP1/2 is kept inactive by the carboxyl tail, possibly by changes in confirmation or destabilization, when not bound to capsids via pUL25.

In addition to nuclear rim localization, 9% of cells transiently expressing GFP-VP1/2ΔR7 (n = 548) displayed remarkable cytoplasmic transport of diffraction-limited fluorescent punctae (Figure 2A; Movie S1). GFP-VP1/2ΔR7 punctae moved along curvilinear trajectories at average velocities of 1.15 mm/s (SD = 0.02; n > 600 runs) (Figure S1A). This movement was sensitive to the microtubule depolymerizing agent nocodazole but not to the actin depolymerizing agent cytochalasin D (Figure S1B). As with the observed nuclear rim localization of GFP-VP1/2ΔR7, microtubule-dependent transport was reminiscent of events that capsids undergo upon entering cells (Sodeik et al., 1997).

To determine if motility occurred by a mechanism that was capable of moving large cargoes through the cytosol, GFP-VP1/2ΔR7 was fused to a membrane targeting sequence (MTS) that anchors proteins to the exterior of mitochondria (Hoogenraad et al., 2003; Pistor et al., 1994). The N terminus of the Bicaudal D protein (BICD-N), which binds dynein/dynactin, redistributes mitochondria to the microtubule-organizing center (MTOC) when fused to a MTS (Hoogenraad et al., 2003). For the following experiments, a GFP-BICD-N-MTS fusion served as a positive control for redistribution of mitochondria to the MTOC, and a GFP-MTS was the negative control. Each MTS-tagged protein colocalized with mitochondria in transfected cells (Figure 2B). GFP-VP1/2ΔR7-MTS induced perinuclear clustering of mitochondria in 37% of transfected cells, which was greater than the negative control (10%, $p = 0.00014$), although not as effective as the BICD-N construct (76%, $p < 0.00001$) (Figures 2B and 2C). A pUL25-GFP-MTS fusion protein redistributed mitochondria only in the presence of full-length VP1/2, confirming that VP1/2 and pUL25 formed a complex that induced cargo transport (Figures 2B and 2C). Full-length VP1/2 lacking a MTS tag did not redistribute mitochondria, indicating that VP1/2 expression did not affect mitochondrial localization indirectly (Figure 2C). In all cases perinuclear clustering of mitochondria was nocodazole sensitive (Figures S1C–S1E). These experiments document the capacity of VP1/2 to move cargo under load by a microtubule-dependent transport process in intact cells and further demonstrate that this property was masked in the full-length VP1/2 protein in the absence of its capsid-binding partner, pUL25.

VP1/2 Interacts with the Dynein/Dynactin Motor Complex

The ability of VP1/2 to move on microtubules and redistribute mitochondria to the perinuclear region of cells led us to examine whether VP1/2 could interact with components of the minus-end-directed]dynein/dynactin microtubule motor complex. To test this possibility, GFP-VP1/2 was immunoprecipitated from transiently transfected HEK293 cells and probed for the presence of the dynein intermediate chain and the p150/glued dynactin subunit. Unexpectedly, full-length VP1/2 coimmunoprecipitated both dynein/dynactin components despite it likely being in an inactive conformation (Figure 3B). Because the interaction with p150/glued proved robust, it was used to examine the VP1/ 2-dynein/ dynactin interaction in more detail. GFP-VP1/2 lacking region 7 coimmunoprecipitated dynactin at 79% ± 49% (mean ± SD; n = 3) of the efficiency of full-length GFP-VP1/2 (Figure 3C). Because VP1/2ΔR7 actively engaged in microtubule-dependent transport, it was used to identify additional regions required for binding dynactin proteins by introducing a series of in-frame deletions (Figure 3A). Individual in-frame deletions of regions 1–5 did not diminish the interaction between VP1/2ΔR7 and dynactin components p150/glued and p50/dynamitin (Figure 3D). In contrast, a GFP-VP1/2ΔR6ΔR7 truncation was severely compromised for binding, as was a variant of GFP-VP1/2ΔR7 deleted for a subregion of region 6, referred to here as $R6^S$ (aa 2080–2796) (Figure 3E). The $\Delta R6^S$ allele was based on a previously described in-frame deletion that attenuated, but did not prevent, PRV propagation (Böttcher et al., 2006). Because expression of GFP-VP1/ 2ΔR6ΔR7 and GFP-VP1/2$\Delta R6^S$ΔR7 was restricted to the nucleus, variants of these isoforms lacking an endogenous nuclear localization sequence were also examined to rule out that nuclear targeting contributed to the reduction of p150/ glued and p50/dynamitin binding (Figures 3E and S2A) (Abaitua and O'Hare, 2008).

Although VP1/2 regions 1–4 in the GFP-VP1/2ΔR7 construct were individually dispensable for the interaction with dynactin proteins, a single deletion of regions 1–4 resulted in a 5-fold (p150/ glued) and 9-fold (p50/dynamitin) decrease in binding when the C terminus was intact (Figure 3F). Deletion of regions 1–5 only incrementally reduced binding in comparison to deletion of regions 1–4: 8-fold (p150/glued) and 11-fold (p50/dynamitin). While additional studies will be required to understand the full extent of the VP1/2-dynactin interaction, the C-terminal third of VP1/2 (consisting of regions 6 and 7) was the smallest fragment identified that was sufficient for the dynactin interaction (Figure 3F). The minimal VP1/2 regions 6 and 7 construct also cosedimented with endogenous dynein/dynactin from transiently]overexpressing cells (Figures S2B and S2C). While this latter approach did not conclusively document an interaction with the 20S dynein motor, the findings supported those obtained by coimmunoprecipitation and the motility observed in transfected cells.

When the region 6^S deletion was combined with deletion of regions 1–4, binding to dynactin was nearly eliminated (19-fold decrease in p150/glued binding and 23-fold decrease in p50/ dynamitin binding). In the context of full-length VP1/2, deletion of region 6^S significantly decreased binding to p150/glued (5-fold decrease, $p = 0.00015$) and p50/dynamitin (4-fold decrease, $p = 0.0005$) (Figure 3F). These findings indicated that region 6^S along with sequences within regions 1–4 contributed to binding individual protein components of dynactin. Collectively, results from coimmunoprecipitation and cosedimentation were consistent with a functional VP1/2-dynein/ dynactin interaction and with the robust microtubule-based motility observed in living cells. Regions 2–7 cannot be individually deleted from VP1/2 without ablating PRV propagation; however, PRV lacking region 6^S is viable (Böttcher et al., 2006; Lee et al., 2006). Therefore, the effect of deleting region 6^S on the cytoplasmic transport of PRV capsids during infection was next examined.

Deletion of the VP1/2 Proline-Rich Sequences Impairs PRV Retrograde Axon Transport in Cultured Sensory Neurons

To analyze PRV retrograde intracellular transport, PRV encoding a fluorescent-capsid reporter (mRFP1-VP26 fusion) and either wild-type VP1/2 (WT), VP1/2ΔR6^S (MUT), or repaired VP1/2 (VP1/2ΔR6^S > WT VP1/2; REP) were isolated. Single-step growth of the MUT virus was initially delayed relative to the WT and REP viruses and plaque diameters were reduced, which was consistent with a trafficking defect (Figures 4A and 4B). Although VP1/2 is essential for virion assembly, there was no reduction in the incorporation of seven structural proteins in the MUT virus and only a statistically insignificant change in particle:plaque-forming unit (pfu) was measured (Figure S3).

To determine the effect of the VP1/2ΔR6^S allele on retrograde axon transport, primary dorsal root ganglion (DRG) sensory neurons were infected with WT, REP,or MUT viruses, and capsid transport events were captured by time-lapse fluorescence imaging prior to 1 hr postinfection (hpi) (Figure 5A). WT and MUT viruses entered axons at equal frequency based on the measured flux of retrograde transport events in excess of 5 mm observed at the distal axons: WT = 0.70 ± 0.07 (moving particles/recording ± SD; n = 261); MUT = 0.67 ± 0.08 (moving particles/recording ± SD; n = 187). Transport dynamics were further surveyed mid-axon by measuring the lengths and average velocities of continuous retrograde transport events, termed runs. PRV lacking region 6^S maintained wild-type retrograde transport velocities, indicating that dynein recruitment to incoming capsids remained in tact (Figures 5B and 5D); however, the MUT virus showed a small shift toward shorter runs (Figures 5C and 5E). Moreover, capsids of the MUT virus displayed an increase in short-lived reversal events that were similar to those normally seen during wild-type infection at lower frequency. While these transient reversals did not manifest as sustained anterograde transport events, they contributed to the reduced efficiency of retrograde transport (Figure 5F).

The changes in retrograde transport dynamics exhibited by the MUT virus predicted that the proline-rich sequences of region 6^S contributed to the efficient delivery of capsids from axon terminals to the nucleus. If correct, the changes in retrograde transport dynamics should translate into a greater overall deficit when measured across the entire length of an axon. To test this prediction, an assay was developed to measure the efficiency of nuclear delivery following retrograde axon transport. DRG explants were coinfected at equal multiplicity with PRV encoding a capsid tagged with either a green or red fluorescent protein (GFP-pUL25 or mCherry-pUL25), and images of sensory neurons within the explant were captured at 2–3 hpi to determine the proportion of green and red capsid accumulation at nuclear rims (Figure 6A). Neuronal soma embedded within intact ganglia are surrounded by support cells and are not expected to be directly exposed to viral inoculum, allowing for differences in retrograde axon transport to be detected. Because the accuracy of the assay required the strict adherence of equal multiplicity for the two reporter viruses, the viral stocks were individually titered prior to the study, and the titer of the combined inoculum used to infect the explants was subsequently reconfirmed. Neuron imaging experiments that were initiated with a combined inoculum in which the two viruses differed in titer by more than 2-fold were discarded from the final analysis. The WT virus accumulated at the nuclear membrane more effectively than the MUT virus (Figure 6B). This result was independent of which virus encoded the red or green fusion tag (Figure 6C). In contrast, coinfection of two WT viruses produced similar amounts of capsid accumulation at nuclear membranes (Figure 6D). In summary, changes in retrograde transport kinetics associated with the VP1/2ΔR6^S allele correlated with a defect in capsid delivery to neuronal nuclei. Based on these results, the phenotype associated with the VP1/ 2ΔR6^S allele was next examined in vivo.

Deletion of the VP1/2 Proline-Rich Sequences Impairs PRV Virulence and Retrograde Axon Transport In Vivo

The goal of the following studies was to determine the time of PRV transmission from a peripheral inoculation site to neuronal somas of the peripheral and central nervous system (PNS and CNS, respectively). Because PRV encoding a deletion equivalent to the VP1/2ΔR6^S allele was previously noted to exhibit reduced virulence in a mouse intranasal infection model, an equivalent study was first performed by inoculating the WT, MUT, and REP reporter viruses intranasally into mice and measuring mean survival times (Figure 4C) (Böttcher et al., 2007). Mice infected with WT virus developed clinical symptoms 2 days postinfection (dpi) and died at an average time of 73 hpi. Similar results were obtained when mice were infected with REP virus. These results match those previously reported for PRV encoding fluorescent protein fusions to the VP26 capsid protein (Bohannon et al., 2012). Symptoms of infection were first noted inmice infected with MUT PRV at 5–6 dpi, with an average time to death of 139 hr (n = 4). One mouse infected with the MUT virus did not develop symptoms prior to the termination of the experiment at 3 weeks postinfection and was not included in the analysis. Thus, consistent with a previous report, deletion of VP1/2 region 6^S decreased virulence of PRV in a mouse model (Böttcher et al., 2007). However, these data did not provide an indication if attenuation was due to a deficit in retrograde axon transport.

To focus specifically on the retrograde transport component of neuroinvasion, an established intraocular infection model was used (Pickard et al., 2002). MUT or REP PRV encoding red capsids (mRFP1-VP26 fusion) were injected unilaterally into a rat eye anterior chamber (Figure 7A). Animals were sacrificed at varying times postinfection to examine the presence of virus fluorescence in the PNS and CNS. Intraocular smooth muscles of the iris and ciliary body receive sympathetic and parasympa- thetic innervation, and these autonomic circuits become infected after virus injection into the anterior chamber of the eye (Figure 7A) (Lee et al., 2009; Pickard et al., 2002). Invasion of the sympathetic retrograde circuit was monitored in the superior cervical ganglion (SCG) of the PNS and downstream in the paraventricular nucleus (PVN) of the CNS. The SCG consists of first-order neurons projecting axons to the iris; the PVN consists of third-order neurons that project axons to preganglionic spinal cord neurons of the intermediolateral nucleus (IML), which in turn project axons to the SCG. Invasion of the parasympathetic retrograde circuit was monitored in the Edinger-Westphal (EW) nucleus of the CNS, which consists of preganglionic second-order neurons that project to the ciliary ganglion (CG) of the PNS, which in turn project to the iris and ciliary body (Figure 7A). The neuron populations included in the analysis were chosen based on the dependence on retrograde transport to produce infection and for ease of isolation and imaging. Infected neurons in the SCG, PVN, and EW were quantified by counting all cells expressing punctate intranuclear red fluorescence indicative of capsid assemblies (Desai et al., 1998; Lee et al., 2009). In all instances, the MUT virus was delayed in invasion of retrograde circuitry relative to the REP virus (Figures 7B–7D). Neuroinvasion is a complex multifactorial phenotype, but nonetheless the in vivo results mimic those obtained in cultured DRG sensory explants and support the model that the proline-rich sequences in VP1/ 2 enhance retrograde axon transport by contributing to the recruitment of the dynactin complex to capsids, thereby promoting dissemination into the nervous system.

DISCUSSION

Upon entering cells many viruses engage microtubule motors to overcome the diffusion barrier of the cytoplasm (Luby-Phelps, 2000). Surprisingly, these viral-host interactions often produce nondirected motion. In the case of adenovirus, capsids participate in minus-end (retrograde) and plus-end (anterograde) directed motion at approximately equal frequency, resulting in random motions that collectively produce only small changes in net

displacement (Gazzola et al., 2009; Suomalainen et al., 1999). This dynamic indicates that facilitated diffusion is sufficient to produce favorable odds that an adenovirus capsid will arrive at its destination (i.e., a nuclear pore); targeted motion may notbe necessary for productive infection. For neuroinvasive viruses, facilitated diffusion alone cannot account for the trafficking of viral particles from axon nerve endings to neural soma that routinely occurs over the scale of centimeters. There has been very little insight garnered regarding how neuroinvasive herpesviruses, such as HSV and PRV, recruit the dynein microtubule motor and produce the highly directed and sustained retrograde motion that is observed in axons of infected neurons (Antinone and Smith, 2010; Smith et al., 2004).

Dynein is the minus-end-directed microtubule motor that is responsible for processive retrograde transport of cytoplasmic cargoes in mammalian cells (reviewed in Vallee et al., 2004). Consistent with this critical function, many viruses recruit dynein to presumably facilitate nuclear delivery (Bremner et al., 2009; Döhner et al., 2002, 2006; Suikkanen et al., 2003). While the mechanism of dynein recruitment is not well understood for any virus, there is increasing evidence that nonenveloped viruses, including adenovirus and papilloma virus, undergo conformational changes upon entry that expose minor capsid proteins that can bind dynein (Florin et al., 2006; Schneider et al., 2011; Wodrich et al., 2010). Whether the intrinsic activities of these proteins are responsible specifically for dynein-based transport during infection has proven difficult to determine, and evidence for alternative mechanisms of dynein recruitment are documented (Bremner et al., 2009).

Herpesvirus entry into cells by membrane fusion results in the deposition of the capsid entry complex into the cytosol. While several tegument proteins are dispensable for retrograde transport, the role of the VP1/2 tegument component of the entry complex has remained untested, as virions fail to assemble in the absence of the protein (Antinone et al., 2006; Desai, 2000; Fuchs et al., 2004). HSV capsid-tegument complexes bind to dynein, kinesins, and dynactin in vitro, and mutations in VP1/2 interfere with capsid delivery to nuclear pores (Abaitua et al., 2012; Radtke et al., 2010; Schipke et al., 2012). Together, these findings support a possible role for VP1/2 in microtubule transport.

The current study documents that VP1/2 is a microtubule transport effector based on the following evidence: (1) VP1/2 associates with constituents of dynein and dynactin and cosediments with dynein/dynactin complexes, (2) VP1/2 engages in rapid and processive microtubule transport in the absence of other viral proteins, and (3) VP1/2 moves large surrogate cargoes through the cytoplasm. Mutants of PRV were isolated to determine if these intrinsic activities contributed to retrograde transport during infection. Because transport following entry could not be studied with a knockout virus, mapping studies were instead used to identify regions of VP1/2 that contributed to the dynactin interaction. The dynactin complex enhances the processivity of the dynein motor and, interestingly, is recruited to capsid-tegument complexes independent of dynein (Kardon et al., 2009; King and Schroer, 2000; Radtke et al., 2010). We hypothesized that dynactin may serve to sustain the longdistance retrograde capsid motion important for axon transport and that mutants with impaired dynactin binding may remain viable.

Although binding to dynactin proved to be complex, with multiple regions of VP1/2 contributing to the interaction, a large proline-rich sequence located in the C-terminal half of the protein was identified as one determinant. In agreement with a previous report, PRV carrying an in-frame deletion of the proline-rich region coding sequence (VP1/2ΔR6^{S}) was viable, allowing for an assessment of VP1/2 function following entry into cells (Böttcher et al., 2006). The VP1/2ΔR6^{S} mutant transported at wild-type retrograde velocity, but over shorter distances compared to PRV encoding wild-type VP1/2, consistent with dynactin serving to enhance the processivity of capsid motion. When cultured neurons were

coinfected with PRV encoding either wild-type VP1/2 or VP1/2ΔR6^S, the wild-type viruses outran the mutants. This result provided an independent confirmation of the transport defect and further demonstrated that the defective instantaneous dynamics of capsid motion observed over short distances were amplified over the full length of the axon. In a final test, viruses encoding VP1/2ΔR6^S were slower at transporting in rat autonomic retrograde circuits. This decrease in neuroinvasion kinetics correlated with a decreased virulence in a mouse intranasal infection model that requires retrograde axon transport for neuroinvasion (Babic et al., 1994). While it was not possible to ascribe causality of the retrograde kinetic defect observed in culture to the delay in neuroinvasion observed in vivo, the results were nevertheless consistent with a role for VP1/2 and dynactin recruitment in prolonged retrograde capsid transport in axons, neuroinvasion, and pathogenesis.

These studies provide insights into mechanisms underlying herpesvirus intracellular transport and neuroinvasion. In addition to these functions, the VP1/2 tegument protein is recognized for its critical roles in genome injection through nuclear pores and subsequently in the assembly and egress of progeny virions (Batterson et al., 1983; Desai, 2000). The protein is regulated during both stages of infection by proteolytic processing (Jovasevic et al., 2008; Leelawong et al., 2012). In contrast, the microtubule transport effector functions of VP1/2 were regulated by an interaction with the capsid protein, pUL25. Because removal of the pUL25 C-terminal binding site in VP1/2 resulted in constitutive and robust microtubule motion, we suggest that the C terminus maintains VP1/2 in an inactive confirmation that can be relieved by the pUL25 interaction. This model predicts that during infection newly translated VP1/2 would remain inactive until becoming capsid bound. How the proline-rich region enhances the dynactin interaction is not clear, but its predicted disordered structure may contribute to conformational changes, indirectly affecting dynactin recruitment (Böttcher et al., 2006). In a similar vein, the proline-rich region of the cellular tau protein enhances binding of microtubules (Goode et al., 1997). Alternatively, the disordered proline-rich sequence may recruit dynactin by mimicking a misfolded protein that normally would be moved to the MTOC by dynein/dynactin (reviewed in Wileman, 2007). VP1/2 is also implicated in recruiting the kinesin motor to enveloped cytoplasmic viral particles late in infection (Shanda and Wilson, 2008). Understanding how VP1/2 coordinates dynein and kinesin throughout infection will be of particular interest.

VP1/2 is noted for its deubiquitinase activity resulting from a cysteine protease domain in the N terminus (Schlieker et al., 2005). In PRV, mutation of the catalytic cysteine of the protease domain results in loss of neuroinvasion in vivo without perturbing viral replication in somatic tissues (Lee et al., 2009). Because the VP1/2ΔR6^S mutant of PRV presented to a lesser extent a neuroinvasive defect in the same in vivo infection model, the possibility that VP1/2 orchestrates a series of steps that contribute to neu-roinvasion seems reasonable. In summary, we document that VP1/2 is a herpesvirus effector of retrograde microtubule transport that enhances neuroinvasion by recruiting the dynactin complex.

EXPERIMENTAL PROCEDURES

Cells and Virus Propagation

Vero (African green monkey kidney epithelial), HEK293 (human embryonic kidney), and PK15 (pig kidney epithelial) cells were grown in DMEM (Dulbec-co's modified Eagle's medium, Invitrogen) supplemented with 10% BGS (bovine growth supplement, HyClone); BGS levels were reduced to 2% during infection. All recombinant viruses were derived from the pBecker3 infectious clone of PRV-Becker. Infectious clones were transfected into PK15 cells as previously described (Luxton et al., 2005). The resultant stock of virus was passaged once more to create a working stock. Titers of working stocks were obtained by plaque assay as previously described (Smith and Enquist, 1999). Plaque sizes of mRFP1-VP26

encoding viruses were measured by live-cell fluorescence imaging. Vero cells in 6-well trays were infected at a concentration of 100–300 pfu per well. Cells were overlaid with methyl cellulose, and plaques were allowed to expand for 2–3 days. Images of at least 30 isolated plaques from each virus strain were acquired with a Nikon Eclipse TE2000-U inverted microscope and a 0.30 NA 103 objective. The average of two orthogonal diameter measurements was calculated for individual plaques and expressed as a percentage of the diameter of PRV-GS847, which was always tested in parallel. Values reported are an average of three independent experiments. Characterization of virus growth kinetics was previously described (Tirabassi and Enquist, 1998), and further details are provided in the Supplemental Experimental Procedures. Culturing DRG from embryonic chicken (E8) on polyornithine- and laminin-treated coverslips was previously described (Smith, 1998; Smith et al., 2001). Ganglia were cultured in defined DMEM/F12 (Invitrogen, 11039-021) medium for 2 days before viral infection.

Viruses and Plasmids

Plasmids, primers, and cloning details are described in Supplemental Experimental Procedures. The viruses used in this study are listed in Table S1. Primers and plasmids are listed in Tables S2 and S3. Transfections were done using polyethylenimine (PEI, Polysciences, catalog no. 23966) or Lipo-fectamine 2000 (Invitrogen). For some experiments, cells were treated with 10 μ;M nocodazole or 0.5 μ;M cytochalasin D before imaging. Additional details are provided in Supplemental Experimental Procedures.

Coimmunoprecipitation and Western Blot Analysis

HEK293 cells transiently expressing GFP and GFP-tagged VP1/2 mutants were treated with 10 μ;M nocodazole (VWR) for 1 hr, washed once with cold PBS supplemented with 0.1 mM phenylmethylsulfonyl fluoride, and lysed 18–24 hr posttransfection in 500 μl/well of cold TAP lysis buffer supplemented with 10 μM nocodazole, 1 mM dithiothreitol, and phosphatase and protease inhibitors. Sepharose A/G beads were loaded with anti-GFP antibodies, washed three times with cold TAP lysis buffer, and incubated with precleared lysates overnight at 4°C. The beads were washed four times and resuspended in loading buffer. Samples were heated at 75°C for 20 min, separated on sodium dodecyl sulfate-polyacrylamide gel, and transferred to PVDF Hybond-P membranes (GE Healthcare). Membranes were blocked and incubated with primary antibody at 4°C overnight. Following incubation with a horseradish peroxidase-conjugated goat anti-mouse antibody (Jackson ImmunoResearch), the blots were processed for chemiluminescence and quantitated by densitometry. The efficiency of protein interaction was described as the ratio of coimmunoprecipitated protein to primary immuno-precipitated protein.

Microscopes and Imaging

Live-cell images were acquired with a Nikon Eclipse TE2000 inverted wide-field fluorescence microscope fitted with a 60 × 1.40 NA oil objective and either a Photometrics CoolSnap HQ2 or a Cascade 650 charge-coupled device (Photometrics, Roper Scientific). All microscopes were housed in a 37°C environmental box (In Vivo Scientific), and infected or transfected cells were imaged in VALAB (Vaseline, lanolin, and beeswax) sealed chambers as previously described (Smith et al., 2001). Mitochondria were stained with MitoTracker Red CMXRos (1:10,000; Invitrogen) according to the manufacturer's protocol.

Analysis of viral particle movement was described previously (Bohannon et al., 2012). To determine the efficiency of virus delivery to the nuclear rim, 2-day-old DRG explants were coinfected with two viruses. Because the accuracy of the assay readout required strict adherence of equal multiplicity for the reporter virus pairs, the viral stocks were titered both before and after infection of the explants. The stocks were thawed, sonicated, and

centrifuged at 3003×*g* for 5 min at room temperature to eliminate cell debris. A mixed stock of the two viruses containing equivalent titers for each virus was prepared and used to infect the DRG. In addition to being used to infect the neurons, the working dilutions of individual prepared viruses were used to confirm the titers of each virus. Neuron imaging experiments that were subsequently determined to have been infected with mixed stocks in which the two viruses differed in titer by more than 2-fold were discarded from the final analysis. Static images from multiple infected neurons were captured 2–3 hr postinfection with sequential RFP and GFP exposures. The three infection pairs were coded and analyzed blindly to determine the most predominant virus color present at specific nuclear rims. Results are presented as the averages of > 5 experiments for each virus combination. The frequency of capsid retrograde transport events (flux) was measured in distal axons of DRG. Two sets of three DRG explants were cultured for 2 days and infected at equal moi with either wild-type or mutant virus (VP1/2ΔR6^S). Each virus stock was thawed, sonicated, and centrifuged at 3003×*g* for 5 min at RTto eliminate cell debris before infection. Viral stocks were titered before and after the experiment as described above. Distal axons were imaged between 10 and 45 min postinfection. In total, 187 movies were recorded for the mutant virus and 261 movies were recorded for wild-type virus. Particle entry flux was determined as the number of moving particles per recording. In order to be scored, particles had to travel at least 5 μm. Additional details are provided in Supplemental Experimental Procedures.

Animal Studies

Animals (CD-1 mice and Long-Evans rats, males, Charles River Breeding Laboratories) were maintained under 12 hr light:12 hr dark conditions throughout with food and water continuously available. All procedures conformed to NIH guidelines for work with laboratory animals and were approved by the Institutional Animal Care and Use Committee of the University of Nebraska, Lincoln. Intranasal infection of CD-1 mice was previously described (Bohannon et al., 2012). Intraocular injections of male Long-Evans rats, isolation of nervous tissues, and processing for fluorescence imaging were previously described (Lee et al., 2009). Further details of both protocols are provided in Supplemental Experimental Procedures.

Statistical Analysis

Statistical significance was determined by unpaired two-tailed Student’s t test for pairwise comparisons. For comparison of multiple experimental groups to a control, a one-way analysis of variance (ANOVA) was performed with a post hoc Tukey’s test.

Supplementary Material

Refer to Web version on PubMed Central for supplementary material.

Acknowledgments

We thank Jenifer Klabis and Gina Daniel for producing recombinants of PRV used in these studies; Anna Akhmanova for constructs used in the mitochondrial experiments; and Duncan Wilson, Chris Wiethoff, and Mark Mandel for insightful discussions and suggestions. This work was funded by NIH grant R01 AI056346 to G.A.S. and R01 EY017809 to G.E.P. and P.J.S. K.P.B. received support from the training program in Immunology and Molecular Pathogenesis from the National Institutes of Health (T32AI07476).

REFERENCES

Abaitua F, O’Hare P. Identification of a highly conserved, functional nuclear localization signal within the N-terminal region of herpes simplex virus type 1 VP1-2 tegument protein. J. Virol. 2008; 82:5234–5244. [PubMed: 18385239]

Abaitua F, Hollinshead M, Bolstad M, Crump CM, O'Hare P. A Nuclear localization signal in herpesvirus protein VP1-2 is essential for infection via capsid routing to the nuclear pore. J. Virol. 2012; 86:8998–9014. [PubMed: 22718835]

Antinone SE, Smith GA. Retrograde axon transport of herpes simplex virus and pseudorabies virus: a live-cell comparative analysis. J. Virol. 2010; 84:1504–1512. [PubMed: 19923187]

Antinone SE, Shubeita GT, Coller KE, Lee JI, Haverlock-Moyns S, Gross SP, Smith GA. The Herpesvirus capsid surface protein, VP26, and the majority of the tegument proteins are dispensable for capsid transport toward the nucleus. J. Virol. 2006; 80:5494–5498. [PubMed: 16699029]

Babic N, Mettenleiter TC, Ugolini G, Flamand A, Coulon P. Propagation of pseudorabies virus in the nervous system of the mouse after intranasal inoculation. Virology. 1994; 204:616–625. [PubMed: 7941329]

Batterson W, Furlong D, Roizman B. Molecular genetics of herpes simplex virus. VIII. further characterization of a temperature-sensitive mutant defective in release of viral DNA and in other stages of the viral reproductive cycle. J. Virol. 1983; 45:397–407. [PubMed: 6296445]

Bohannon KP, Sollars PJ, Pickard GE, Smith GA. Fusion of a fluorescent protein to the pUL25 minor capsid protein of pseudorabies virus allows live-cell capsid imaging with negligible impact on infection. J. Gen. Virol. 2012; 93:124–129. [PubMed: 21976610]

Bosem ME, Harris R, Atherton SS. Optic nerve involvement in viral spread in herpes simplex virus type 1 retinitis. Invest. Ophthalmol. Vis. Sci. 1990; 31:1683–1689. [PubMed: 1698742]

Böttcher S, Klupp BG, Granzow H, Fuchs W, Michael K, Mettenleiter TC. Identification of a 709-amino-acid internal nonessen-tial region within the essential conserved tegument protein (p)UL36 of pseu-dorabies virus. J. Virol. 2006; 80:9910–9915. [PubMed: 16973597]

Böttcher S, Granzow H, Maresch C, Möhl B, Klupp BG, Mettenleiter TC. Identification of functional domains within the essential large tegument protein pUL36 of pseudorabies virus. J. Virol. 2007; 81:13403–13411. [PubMed: 17928337]

Bremner KH, Scherer J, Yi J, Vershinin M, Gross SP, Vallee RB. Adenovirus transport via direct interaction of cytoplasmic dynein with the viral capsid hexon subunit. Cell Host Microbe. 2009; 6:523–535. [PubMed: 20006841]

Cardone G, Newcomb WW, Cheng N, Wingfield PT, Trus BL, Brown JC, Steven AC. The UL36 tegument protein of herpes simplex virus 1 has a composite binding site at the capsid vertices. J. Virol. 2012; 86:4058–4064. [PubMed: 22345483]

Coller KE, Lee JI, Ueda A, Smith GA. The capsid and tegument of the alphaherpesviruses are linked by an interaction between the UL25 and VP1/2 proteins. J. Virol. 2007; 81:11790–11797. [PubMed: 17715218]

Copeland AM, Newcomb WW, Brown JC. Herpes simplex virus replication: roles of viral proteins and nucleoporins in capsid-nucleus attachment. J. Virol. 2009; 83:1660–1668. [PubMed: 19073727]

Delboy MG, Nicola AV. A pre-immediate-early role for tegument ICP0 in the proteasome-dependent entry of herpes simplex virus. J. Virol. 2011; 85:5910–5918. [PubMed: 21471243]

Desai PJ. A null mutation in the UL36 gene of herpes simplex virus type 1 results in accumulation of unenveloped DNA-filled capsids in the cytoplasm of infected cells. J. Virol. 2000; 74:11608–11618. [PubMed: 11090159]

Desai P, DeLuca NA, Person S. Herpes simplex virus type 1 VP26 is not essential for replication in cell culture but influences production of infectious virus in the nervous system of infected mice. Virology. 1998; 247:115–124. [PubMed: 9683577]

Dodding MP, Way M. Coupling viruses to dynein and kinesin-1. EMBO J. 2011; 30:3527–3539. [PubMed: 21878994]

Döhner K, Wolfstein A, Prank U, Echeverri C, Dujardin D, Vallee R, Sodeik B. Function of dynein and dynactin in herpes simplex virus capsid transport. Mol. Biol. Cell. 2002; 13:2795–2809. [PubMed: 12181347]

Döhner K, Radtke K, Schmidt S, Sodeik B. Eclipse phase of herpes simplex virus type 1 infection: Efficient dynein-mediated capsid transport without the small capsid protein VP26. J. Virol. 2006; 80:8211–8224. [PubMed: 16873277]

Douglas MW, Diefenbach RJ, Homa FL, Miranda-Saksena M, Rixon FJ, Vittone V, Byth K, Cunningham AL. Herpes simplex virus type 1 capsid protein VP26 interacts with dynein light

chains RP3 and Tctex1 and plays a role in retrograde cellular transport. J. Biol. Chem. 2004; 279:28522–28530. [PubMed: 15117959]

Enquist LW. Infection of the mammalian nervous system by pseu-dorabies virus (PRV). Seminars in Virology. 1994; 5:221–231.

Florin L, Becker KA, Lambert C, Nowak T, Sapp C, Strand D, Streeck RE, Sapp M. Identification of a dynein interacting domain in the papillomavirus minor capsid protein l2. J. Virol. 2006; 80:6691–6696. [PubMed: 16775357]

Fuchs W, Klupp BG, Granzow H, Mettenleiter TC. Essential function of the pseudorabies virus UL36 gene product is independent of its interaction with the UL37 protein. J. Virol. 2004; 78:11879–11889. [PubMed: 15479829]

Gazzola M, Burckhardt CJ, Bayati B, Engelke M, Greber UF, Koumoutsakos P. A stochastic model for microtubule motors describes the in vivo cytoplasmic transport of human adenovirus. PLoS Comput. Biol. 2009; 5:e1000623. [PubMed: 20041204]

Gibson W, Roizman B. Proteins specified by herpes simplex virus. 8. Characterization and composition of multiple capsid forms of subtypes 1 and 2. J. Virol. 1972; 10:1044–1052. [PubMed: 4344252]

Goode BL, Denis PE, Panda D, Radeke MJ, Miller HP, Wilson L, Feinstein SC. Functional interactions between the proline-rich and repeat regions of tau enhance microtubule binding and assembly. Mol. Biol. Cell. 1997; 8:353–365. [PubMed: 9190213]

Hoogenraad CC, Wulf P, Schiefermeier N, Stepanova T, Galjart N, Small JV, Grosveld F, de Zeeuw CI, Akhmanova A. Bicaudal D induces selective dynein-mediated microtubule minus end-directed transport. EMBO J. 2003; 22:6004–6015. [PubMed: 14609947]

Jovasevic V, Liang L, Roizman B. Proteolytic cleavage of VP1-2 is required for release of herpes simplex virus 1 DNA into the nucleus. J. Virol. 2008; 82:3311–3319. [PubMed: 18216103]

Kardon JR, Reck-Peterson SL, Vale RD. Regulation of the processivity and intracellular localization of Saccharomyces cerevisiae dynein by dynactin. Proc. Natl. Acad. Sci. USA. 2009; 106:5669–5674. [PubMed: 19293377]

King SJ, Schroer TA. Dynactin increases the processivity of the cytoplasmic dynein motor. Nat. Cell Biol. 2000; 2:20–24. [PubMed: 10620802]

Krautwald M, Fuchs W, Klupp BG, Mettenleiter TC. Translocation of incoming pseudorabies virus capsids to the cell nucleus is delayed in the absence of tegument protein pUL37. J. Virol. 2009; 83:3389–3396. [PubMed: 19144717]

Kristensson K, Lycke E, Röyttä M, Svennerholm B, Vahlne A. Neuritic transport of herpes simplex virus in rat sensory neurons in vitro. Effects of substances interacting with microtubular function and axonal flow [nocodazole, taxol and erythro-9-3-(2-hydroxynonyl)adenine]. J. Gen. Virol. 1986; 67:2023–2028. [PubMed: 2427647]

Lee JI, Luxton GW, Smith GA. Identification of an essential domain in the herpesvirus VP1/2 tegument protein: the carboxy terminus directs incorporation into capsid assemblons. J. Virol. 2006; 80:12086–12094. [PubMed: 17005660]

Lee JI, Sollars PJ, Baver SB, Pickard GE, Leelawong M, Smith GA. A herpesvirus encoded deubiquitinase is a novel neuroinvasive determinant. PLoS Pathog. 2009; 5:e1000387. [PubMed: 19381253]

Leelawong M, Lee JI, Smith GA. Nuclear egress of pseudora-bies virus capsids is enhanced by a subspecies of the large tegument protein that is lost upon cytoplasmic maturation. J. Virol. 2012; 86:6303–6314. [PubMed: 22438563]

Luby-Phelps K. Cytoarchitecture and physical properties of cytoplasm: volume, viscosity, diffusion, intracellular surface area. Int. Rev. Cytol. 2000; 192:189–221. [PubMed: 10553280]

Luxton GW, Haverlock S, Coller KE, Antinone SE, Pincetic A, Smith GA. Targeting of herpesvirus capsid transport in axons is coupled to association with specific sets of tegument proteins. Proc. Natl. Acad. Sci. USA. 2005; 102:5832–5837. [PubMed: 15795370]

Morrison EE, Stevenson AJ, Wang YF, Meredith DM. Differences in the intracellular localization and fate of herpes simplex virus tegument proteins early in the infection of Vero cells. J. Gen. Virol. 1998; 79:2517–2528. [PubMed: 9780059]

Ogasawara M, Suzutani T, Yoshida I, Azuma M. Role of the UL25 gene product in packaging DNA into the herpes simplex virus capsid: location of UL25 product in the capsid and demonstration that it binds DNA. J. Virol. 2001; 75:1427–1436. [PubMed: 11152516]

Openshaw H, Stampalia L, Asher LS. Retrograde axoplasmic transport of herpes simplex virus. Trans. Am. Neurol. Assoc. 1978; 103:238–239. [PubMed: 92846]

Pasdeloup D, Blondel D, Isidro AL, Rixon FJ. Herpesvirus capsid association with the nuclear pore complex and viral DNA release involve the nucleoporin CAN/Nup214 and the capsid protein pUL25. J. Virol. 2009; 83:6610–6623. [PubMed: 19386703]

Pickard GE, Smeraski CA, Tomlinson CC, Banfield BW, Kaufman J, Wilcox CL, Enquist LW, Sollars PJ. Intravitreal injection of the attenuated pseudorabies virus PRV Bartha results in infection of the hamster suprachiasmatic nucleus only by retrograde transsynaptic transport via autonomic circuits. J. Neurosci. 2002; 22:2701–2710. [PubMed: 11923435]

Pistor S, Chakraborty T, Niebuhr K, Domann E, Wehland J. The ActA protein of Listeria monocytogenes acts as a nucleator inducing reorganization of the actin cytoskeleton. EMBO J. 1994; 13:758–763. [PubMed: 8112291]

Radtke K, Kieneke D, Wolfstein A, Michael K, Steffen W, Scholz T, Karger A, Sodeik B. Plus- and minus-end directed microtubule motors bind simultaneously to herpes simplex virus capsids using different inner tegument structures. PLoS Pathog. 2010; 6:e1000991. [PubMed: 20628567]

Roberts AP, Abaitua F, O'Hare P, McNab D, Rixon FJ, Pasdeloup D. Differing roles of inner tegument proteins pUL36 and pUL37 during entry of herpes simplex virus type 1. J. Virol. 2009; 83:105–116. [PubMed: 18971278]

Rode K, Döhner K, Binz A, Glass M, Strive T, Bauerfeind R, Sodeik B. Uncoupling uncoating of herpes simplex virus genomes from their nuclear import and gene expression. J. Virol. 2011; 85:4271–4283. [PubMed: 21345968]

Schipke J, Pohlmann A, Diestel R, Binz A, Rudolph K, Nagel CH, Bauerfeind R, Sodeik B. The C terminus of the large tegument protein pUL36 contains multiple capsid binding sites that function differently during assembly and cell entry of herpes simplex virus. J. Virol. 2012; 86:3682–3700. [PubMed: 22258258]

Schlieker C, Korbel GA, Kattenhorn LM, Ploegh HL. A deubiquitinating activity is conserved in the large tegument protein of the her-pesviridae. J. Virol. 2005; 79:15582–15585. [PubMed: 16306630]

Schneider MA, Spoden GA, Florin L, Lambert C. Identification of the dynein light chains required for human papillomavirus infection. Cell. Microbiol. 2011; 13:32–46. [PubMed: 21166973]

Shanda SK, Wilson DW. UL36pisrequired for efficient transport of membrane-associated herpes simplex virus type 1 along microtubules. J. Virol. 2008; 82:7388–7394. [PubMed: 18495763]

Smith, CL. In Culturing nerve cells. Banker, G.; Goslin, K., editors. Cambridge, MA: MIT Press; 1998.

Smith GA, Enquist LW. Construction and transposon mutagen-esis in Escherichia coli of a full-length infectious clone of pseudorabies virus, an alphaherpesvirus. J. Virol. 1999; 73:6405–6414. [PubMed: 10400733]

Smith GA, Gross SP, Enquist LW. Herpesviruses use bidirectional fast-axonal transport to spread in sensory neurons. Proc. Natl. Acad. Sci. USA. 2001; 98:3466–3470. [PubMed: 11248101]

Smith GA, Pomeranz L, Gross SP, Enquist LW. Local modulation of plus-end transport targets herpesvirus entry and egress in sensory axons. Proc. Natl. Acad. Sci. USA. 2004; 101:16034–16039. [PubMed: 15505210]

Sodeik B, Ebersold MW, Helenius A. Microtubule-mediated transport of incoming herpes simplex virus 1 capsids to the nucleus. J. Cell Biol. 1997; 136:1007–1021. [PubMed: 9060466]

Suikkanen S, Aaltonen T, Nevalainen M, Välilehto O, Lindholm L, Vuento M, Vihinen-Ranta M. Exploitation of microtubule cytoskeleton and dynein during parvoviral traffic toward the nucleus. J. Virol. 2003; 77:10270–10279. [PubMed: 12970411]

Suomalainen M, Nakano MY, Keller S, Boucke K, Stidwill RP, Greber UF. Microtubule-dependent plus- and minus end-directed motilities are competing processes for nuclear targeting of adenovirus. J. Cell Biol. 1999; 144:657–672. [PubMed: 10037788]

Szpara ML, Tafuri YR, Parsons L, Shamim SR, Verstrepen KJ, Legendre M, Enquist LW. A wide extent of inter-strain diversity in virulent and vaccine strains of alphaherpesviruses. PLoS Pathog. 2011; 7:e1002282. [PubMed: 22022263]

Tirabassi RS, Enquist LW. Role of envelope protein gE endocy-tosis in the pseudorabies virus life cycle. J. Virol. 1998; 72:4571–4579. [PubMed: 9573220]

Vallee RB, Williams JC, Varma D, Barnhart LE. Dynein: An ancient motor protein involved in multiple modes of transport. J. Neurobiol. 2004; 58:189–200. [PubMed: 14704951]

Wileman T. Aggresomes and pericentriolar sites of virus assembly: cellular defense or viral design? Annu. Rev. Microbiol. 2007; 61:149–167. [PubMed: 17896875]

Wodrich H, Henaff D, Jammart B, Segura-Morales C, Seelmeir S, Coux O, Ruzsics Z, Wiethoff CM, Kremer EJ. A capsid-encoded PPxY-motif facilitates adenovirus entry. PLoS Pathog. 2010; 6:e1000808. [PubMed: 20333243]

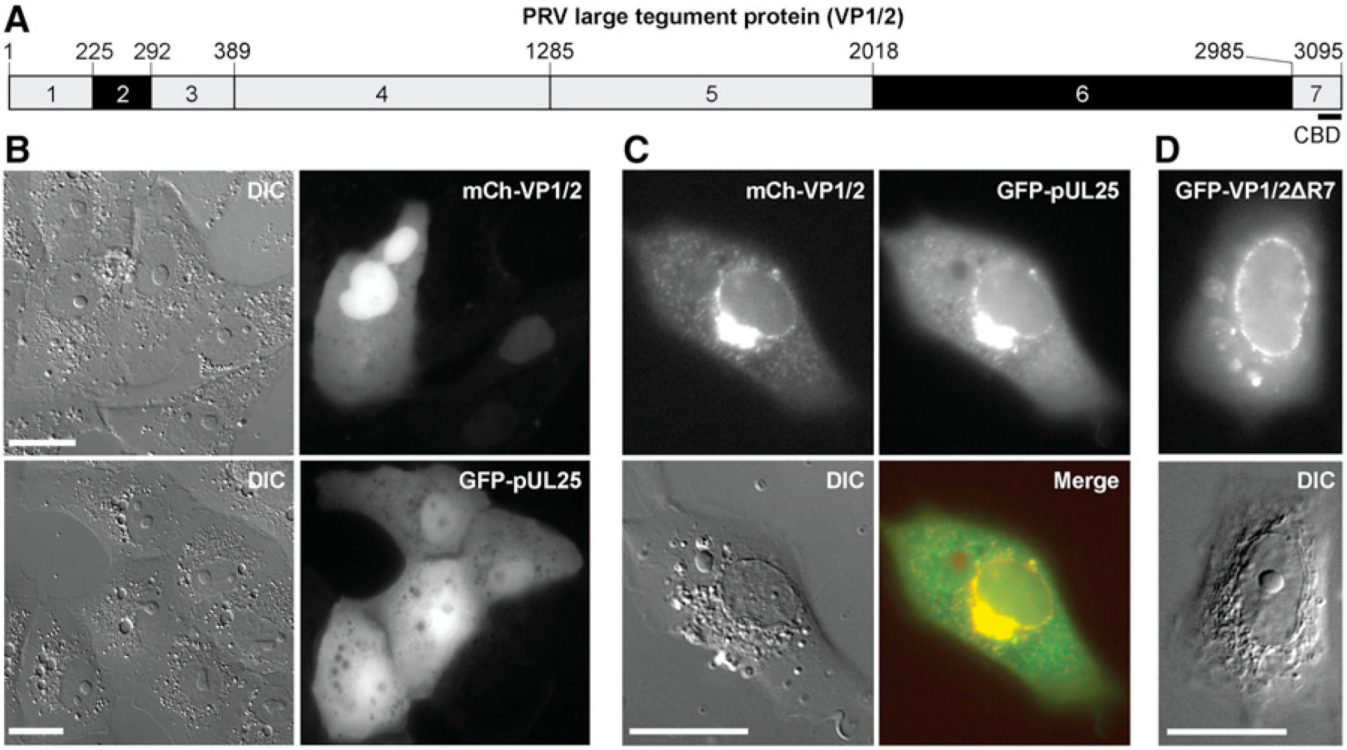

Figure 1. The pUL25 Capsid Protein Unmasks VP1/2 Nuclear Membrane Localization

(A) Schematic representation of seven regions of VP1/2. Regions 2 and 6 are proline rich (black). Position of the capsid binding domain (CBD) consisting of amino acids 3034–3095 is indicated. Amino acid positions based on GenBank JF797219.1 are indicated above the schematic (Szpara et al., 2011).

(B) Transiently expressed mCherry-VP1/2 or GFP-pUL25 were diffuse in Vero cells, with mCherry-VP1/2 often enriched in the nucleus.

(C) Coexpressed mCherry-VP1/2 and GFP-pUL25 were enriched in the perinuclear region and nuclear rim.

(D) VP1/2 localized to the nuclear rim in the absence of pUL25 when the capsid/pUL25 binding domain was removed (ΔR7). Images were captured 18–24 hr posttransfection (hpt). Scale bars are 20 μm.

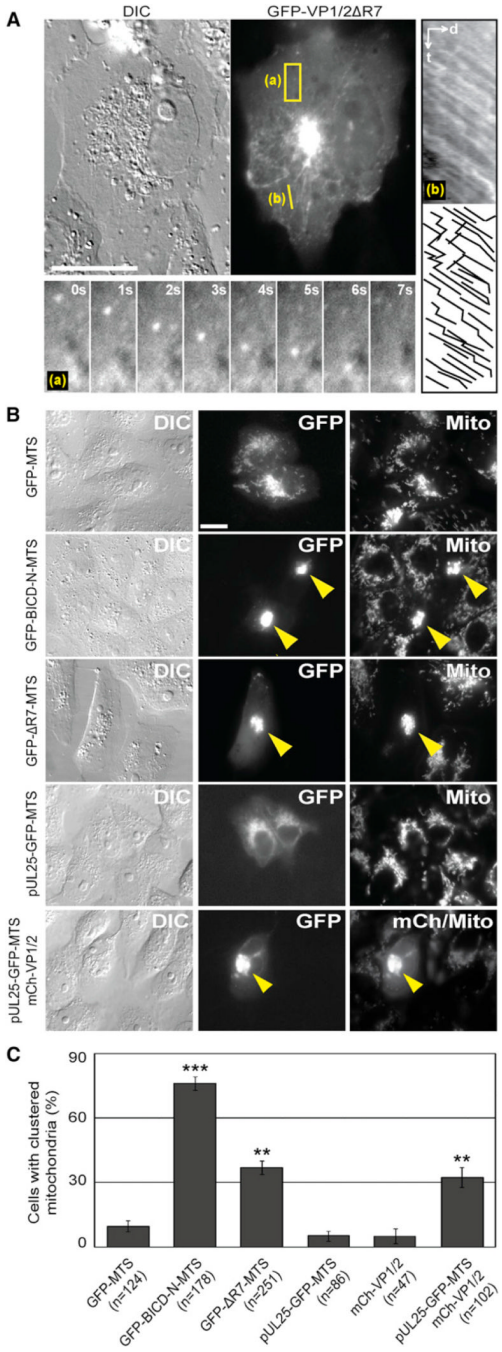

Figure 2. VP1/2 Promotes Microtubule Transport and Is Active Under Load

(A) Transiently expressed GFP-VP1/2ΔR7 moved in curvilinear trajectories and accumulated adjacent to the nucleus in Vero cells. The 3.0 μm × 7.8 μm region denoted (a) is expandedasa time-lapse montage below the image. The 5.6 mm linescan labeled (b) was used to produce the kymograph right of the image. Motion traces are shown below the kymograph (d, distance; t, time).

(B) Anchoring of VP1/2 to the surface of mitochondria promoted organelle redistribution. GFP-VP1/2ΔR7 fused to a membrane targeting sequence that directs association with the outer surface of mitochondria (GFP-ΔR7-MTS) or coexpression of mCherry-VP1/2 and pUL25-GFP-MTS fusions resulted in redistribution of mitochondria to the perinuclear

region of Vero cells (yellow arrowheads). A GFP-MTS fusion served as a negative control and a GFP-BICD-N-MTS fusion as a positive control. Cells were stained with MitoTracker Red to visualize mitochondria.

(C) Summary of mitochondria redistribution results. Values are the percentage of cells with clustered mitochondria ± standard error of the proportion (SEP). Asterisks indicate statistically significant difference from GFP-MTS (***$p < 0.0001$, **$p < 0.001$) as determined by Student's t test. All images (A–C) were captured between 18 and 24 hpt. Scale bars are 20 mm. See also Figure S1 and Movie S1.

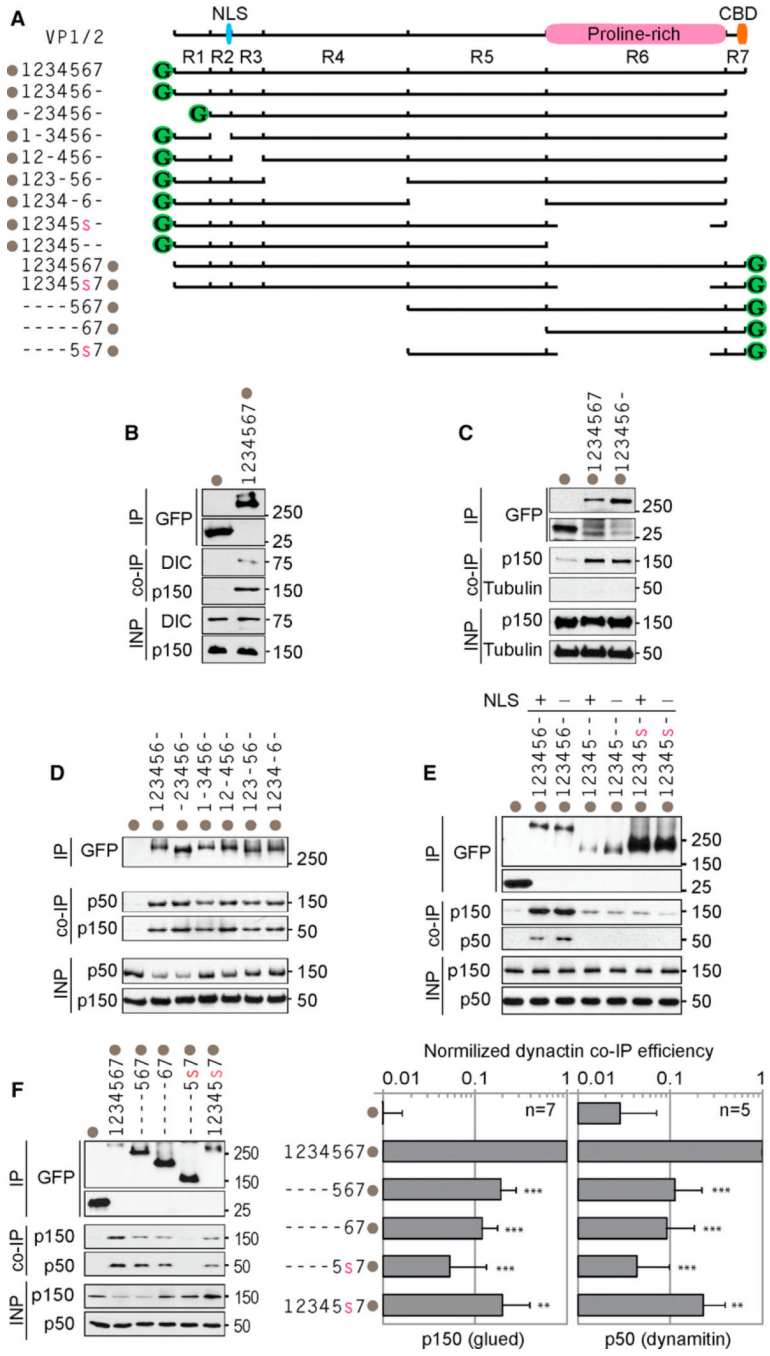

Figure 3. VP1/2 Interacts with Components of the Dynein/Dynactin Complex

(A) Illustration of VP1/2 constructs used for mapping the dynein/dynactin interaction. Locations of proline-rich region, CBD, and cryptic nuclear localization signal (NLS) are indicated at top. Constructs are named for each intact region number with a dash indicating removed regions. The in-frame deletion of a subregion of region 6 is indicated by a red colored lowercase ‘‘s’’ (deletion of amino acids 2087–2796). Gray dots indicate position of the GFP tag for each construct.

(B) Dynein intermediate chain (DIC) and dynactin (p150/glued) coimmunoprecipitated with VP1/2.

(C) VP1/2 region 7 was dispensable for p150/glued coimmunoprecipitation.

(D) Removal of regions 1–5 did not impair dynactin (p50/dynamitin and p150/glued) interaction with VP1/2ΔR7.
(E) VP1/2 region 6^S was required for efficient interaction with dynactin. Mutation of the NLS (K^{285}RRR > AAAA change) did not restore the interaction.
(F) VP1/2 regions 6 and 7 were sufficient for dy-nactin interaction, but regions 1–4 were required for optimal binding. Densitometry plots show normalized p150/glued and p50/dynamitin binding efficiencies. Values in bar graphs (A–F) are averages ± SD. Number of repetitions is indicated (n). Asterisks indicate statistically significant difference from full-length VP1/2-GFP as determined by Student's t test (***$p < 0.0001$, **$p < 0.001$). For all experiments, HEK293 cells were lysed 16–18 hr posttransfection, and VP1/2 was immunoprecipitated with anti-GFP antibody. Coimmunoprecipitated endogenous proteins were detected by western blot. INP, input (6% of crude lysate). See also Figure S2.

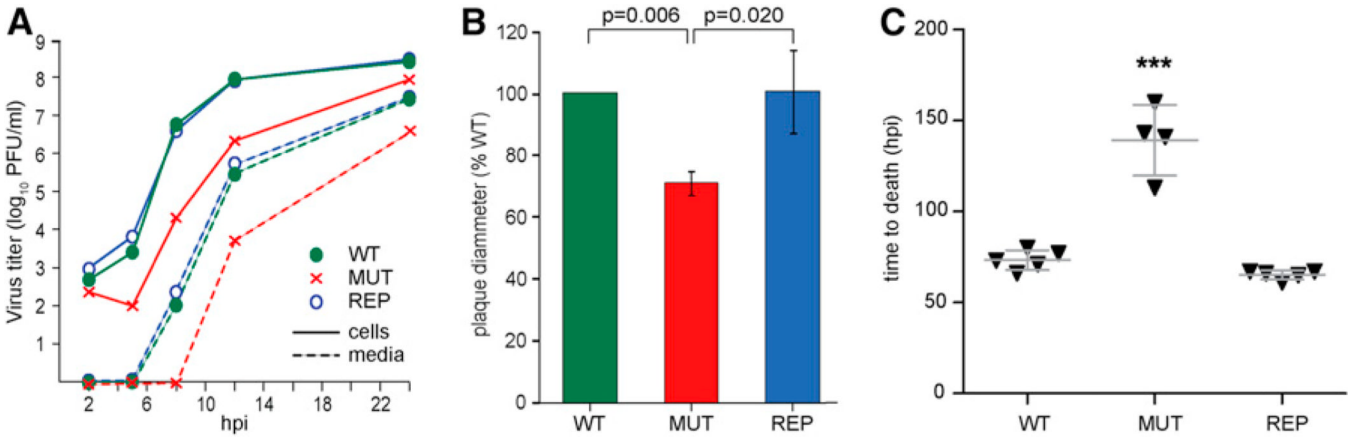

Figure 4. The Proline-Rich Sequences in VP1/2 Region 6 Contribute to Efficient PRV Propagation, Spread, and Virulence

(A) Single-step growth kinetics of PRV encoding either wild-type VP1/2 (WT), VP1/2ΔR6^S (MUT), or repaired VP1/2 (REP). All viruses encode a mRFP1-VP26 fusion (red capsids). Plaque-forming units were quantified from Vero cells (cells) and tissue culture supernatants (media).

(B) Plaque diameters of the MUT and REP viruses were measured in side-by-side experiments with WT virus. A total of 30–70 plaques were analyzed per virus per experiment. Error bars are SD based on three independent experiments. p values were determined by Student's t test.

(C) Mice were infected by intranasal instillation of the WT, MUT, and REP viruses. Each triangle on the scatterplot represents one mouse. Error bars are SD. Asterisks indicate statistically significant difference from WT (***$p < 0.001$) as determined by Tukey's test. See also Figure S3.

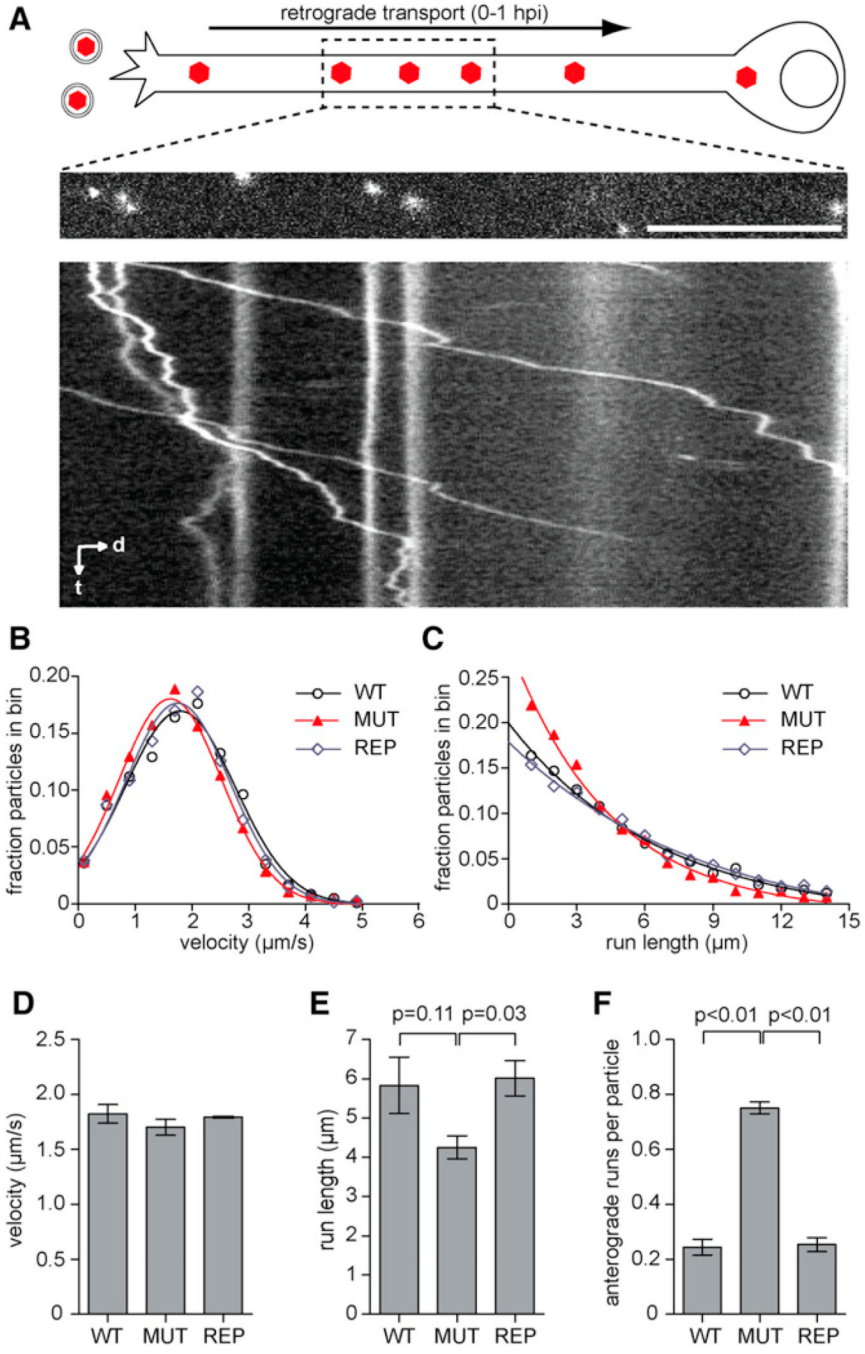

Figure 5. Capsid Transport Dynamics in Sensory Axons

(A–F) DRG explants were infected with the WT, MUT, or REP viruses at 7.0 3 10^6 pfu/coverslip. During the first hour postinfection, moving fluorescent capsids were imaged at 10 frames per second. (A) DRG neuron infected with RFP-capsid tagged virus is illustrated at top. Middle panel is the first frame from a time-lapse recording with the corresponding kymograph aligned below (d, distance; t, time). Scale bar, 10 mm. (B) Profile of capsid retrograde transport velocities. Each data point is an average velocity of a capsid run (uninterrupted period of unidirectional transport). Data were combined from three replicate experiments (n > 80 capsid recordings per experiment). (C) Profile of run lengths. Analyses in (B) and (C) are from the same data set. (D and E) Average velocity and length of

retrograde runs longer than 0.5 mm based on data presented in (B) and (C). (F) Frequency of anterograde runs ≥ 0.5 mm per particle. Error bars are SEM based on three replicate experiments per sample. p values were determined by one-way analysis of variance and a post hoc Tukey's test.

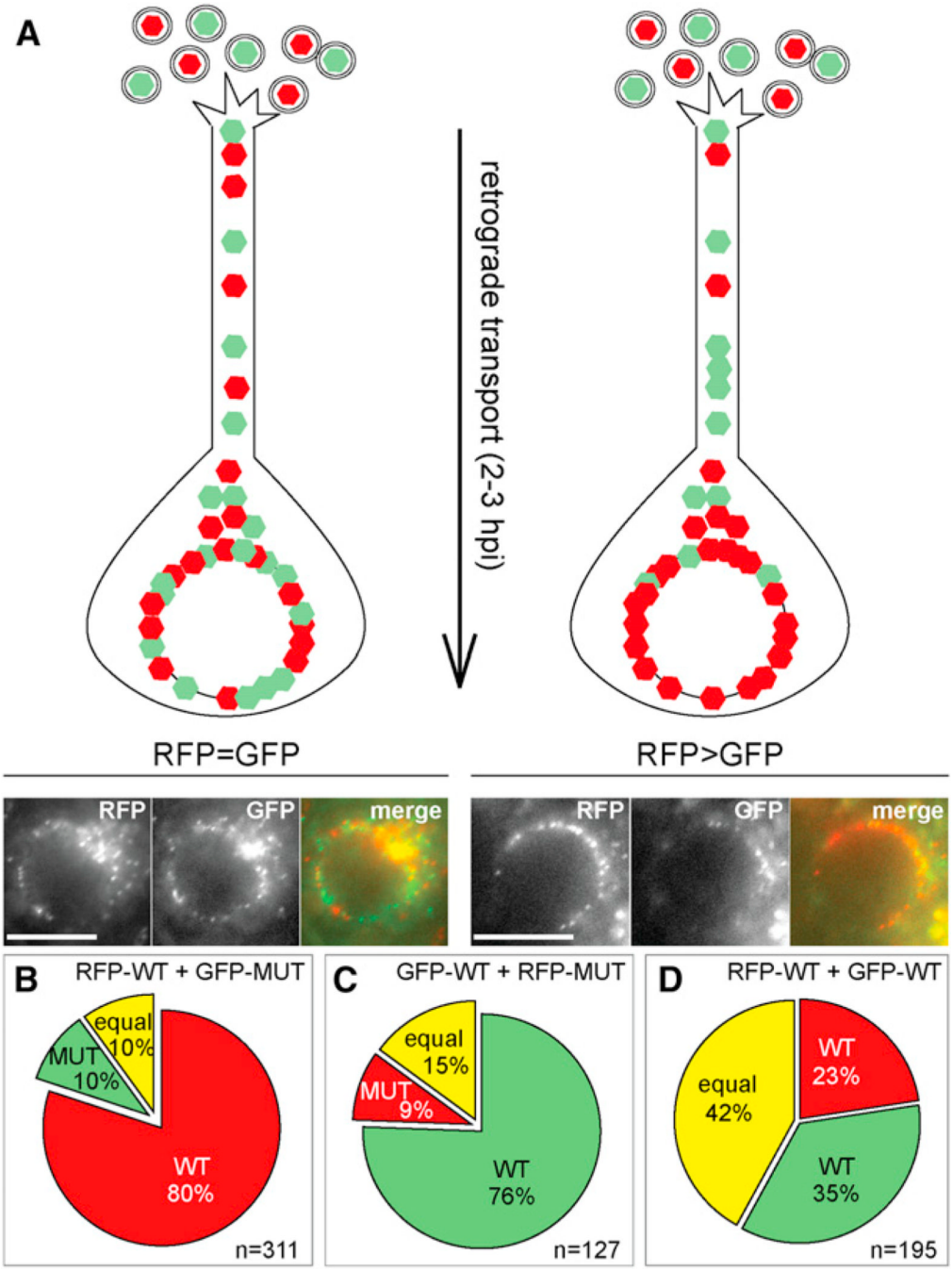

Figure 6. Mutant Virus Was Less Efficient Than WT Virus in Reaching the Nucleus of Explanted DRG

(A–D) DRG were coinfected with equal pfu of two viruses with contrasting fluorophores (mCherry or GFP) fused to pUL25. Illustration of the assay is shown in (A) along with examples of equal distribution of color at the nuclear rim (RFP = GFP) and unequal distribution (RFP > GFP). (B–D) Distribution of capsids at the nuclear rim for WT-MUT (B and C) and WT-WT (D) coinfections. Numbers of analyzed nuclei are indicated (n). Scale bars are 10 μm.

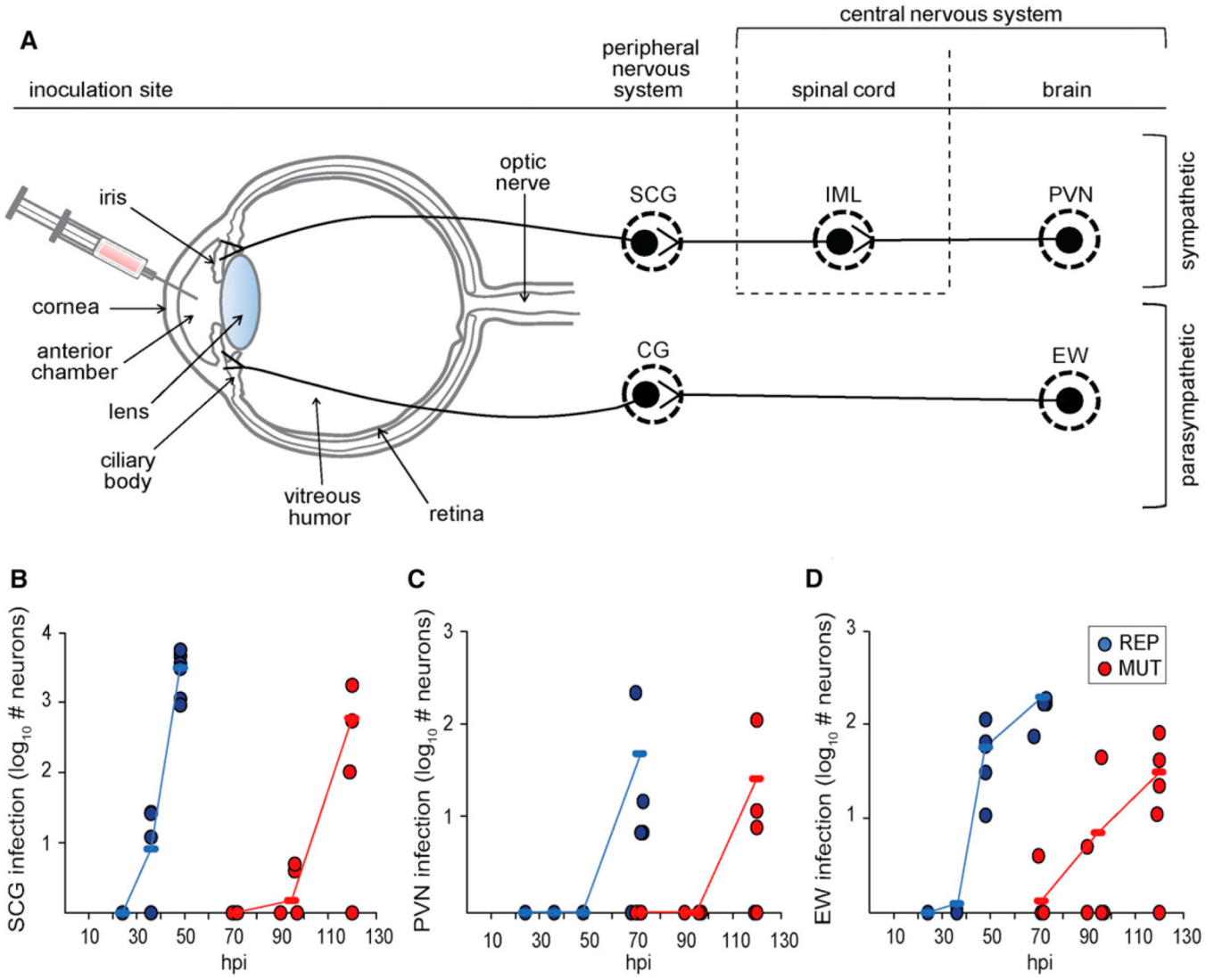

Figure 7. Deletion of VP1/2 Proline-Rich Sequence Delays Neuroinvasion in Retrograde Circuits

(A) Illustration of the rat eye injection model. Virus injected into the anterior chamber is exposed to the ciliary body and iris, which receive sympathetic and parasympathetic input. The sympathetic circuit (top) consists of the superior cervical ganglion (SCG), which receives input from the intermediolateral nucleus (IML), which in turn receives input from the paraventricular nucleus (PVN). The parasympathetic circuit (bottom) consists of the ciliary ganglion (CG), which receives input from the Edinger-Westphal (EW) nucleus. (B–D) Male Long-Evans rats were injected with PRV encoding either VP1/2ΔR6^{S} (MUT) or repaired VP1/2 (REP). All viruses encoded the mRFP1-VP26 fusion (capsid reporter). Each circle on the scatterplot represents a single animal. Animals were sacrificed and fluorescent cells were counted at times indicated. (B), SCG; (C), PVN; (D), EW. Average values are indicated by horizontal dashes and connected to show trends in the data for the mutant virus (red) and the repaired virus (blue).